

Design and Full-Wave Analysis of Cavity-Backed Resistively Loaded Circular-End Bow-Tie Antennas for GPR Applications – Part II

Diego Caratelli and Alexander Yarovoy

Delft University of Technology, IRCTR
Mekelweg 4 – 2628 CD Delft, the Netherlands
d.caratelli@tudelft.nl

Abstract – In this paper, a comprehensive analysis of a novel *GPR* antenna featuring almost 30 : 1 relative bandwidth (55 MHz – >1.5 GHz), with a maximum antenna size of 40 cm is performed. Antenna transient behavior, near-field radiation, and impact of the ground are analyzed in details. It has been shown that the antenna exhibits reduced and short ringing, low spurious energy emission in the air region, as well as stable circuitual and radiation properties over different types of soil. Furthermore, the analysis of buried pipe detection using two such antennas has been performed. Novelty of such investigation lies in the fact that at the lowest operational frequency both the receive antenna and buried pipe are situated in the near-field region, whilst at the highest operational frequency only the far field is playing the role. From this analysis, antenna coupling level and waveforms of the target return, which are of crucial importance for *GPR* system design, are determined.

Index Terms – Antenna coupling, antenna transient behavior, bow-tie antenna, buried pipe, ground-penetrating radar, near-field radiation.

I. INTRODUCTION

In Part II of this paper, the detailed full-wave analysis of the ultra-wideband cavity-backed resistively loaded bow-tie antenna for ground penetrating radars (*GPR*) presented by the authors in [1] and exhibiting almost 30 : 1 relative bandwidth (55 MHz – >1.5 GHz), with a maximum antenna size of 40 cm is carried out. Dielectric

embedding and resistive loading of the radiating structure are used to reduce the flair angle and the antenna size, as well as to assure stable antenna performance over different types of the ground. To reduce parasitic emission to air, the antenna is cavity backed [2–3]. Special cavity filling is suggested in order to keep wideband antenna matching. The specially developed locally conformal finite-difference time-domain (*FDTD*) procedure [1] is used for numerical optimization of the antenna loading profile.

In the case of stepped-frequency continuous-wave (*SFCW*) radar applications (for which the antenna is designed), the synthesis of a pulse in time domain requires the deconvolution of the antenna impulse response [4]. So, antenna features such as the transient behavior and near-field radiation properties have a relevant impact on the performance of a complete *GPR* system, and thus analyzed in details. The proximity effect of the ground may adversely affect the radiation properties and circuitual performance of the antenna [5] and directly affect the antenna impulse response. Thus, ground influence on all antenna characteristics have been studied carefully.

An extensive analysis of the subsurface radar consisting of two identical cavity-backed resistively-loaded bow-tie antennas located above a lossy homogeneous half space where an infinitely-long dielectric pipe is buried is carried out. Novelty of such investigation lies in the fact that at the lowest operational frequency both the receive antenna and the buried pipe are situated in the near-field region, whilst

at the highest operational frequency only the far field is playing the role. The obtained numerical results, also, provide a physical insight into the underlying mechanisms of subsurface diffraction and antenna mutual coupling processes. This information in turn is important to specify the requirements of a complete *GPR* system such as maximal level of the received signal [9–10], system dynamic range, and radiation level in the air region (subject to e.g. *FCC* regulations), as well as to optimize the performance of detection algorithms in terms of clutter rejection.

This paper is organized as follows. Transient behavior of the antenna and its near-field radiation properties are investigated in Sections II and III, respectively. The impact of the ground on the electromagnetic characteristics of the radiator is deeply discussed in Section IV. Finally, Section V presents a thorough analysis of the *GPR* unit in realistic operative scenarios.

II. THE ANTENNA TRANSIENT BEHAVIOR

The time-domain behavior of the electromagnetic field radiated by the structure has been investigated to gain a physical insight into transient emission phenomena responsible for the antenna properties.

Shown in Fig. 1 is the distribution of the y -component of the electric field excited along the H -plane of the antenna (xz -plane), where the other E -field components are vanishing due to the symmetry of the radiating element. The observation points are located at different polar angles θ , along a circle of radius $r_o = 40$ cm, centered at the projection of the feeding point on the air-ground interface. The field component E_y is graphed positive on the side of the time axis for which $\hat{\theta}$ points away from the axis (clockwise direction). The dashed curves marked W_{g_i} ($i = 0, 1, 2, \dots$) and W_{a_j} ($j = 1, 2, \dots$) connect the times of arrival for different wavefronts in the ground and air region, respectively (see Fig. 2). In particular, the curve W_{g_0} related to the radiation process occurring at the feeding point is roughly a circle meaning that, at every observation point in the ground, the radio wave

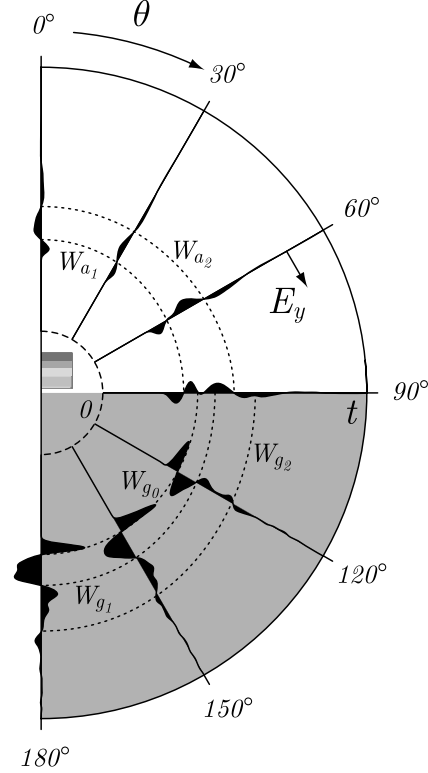


Fig. 1. Time-domain behavior of the electric field radiated along the H -plane of the antenna. The observation points are located at different polar angles θ , along a circle of radius $r_o = 40$ cm, centered at the projection of the feeding point on the air-ground interface.

contribution from the feed arrives at the same time

$$t_{g_0} \simeq t_0 + \frac{r}{c_0} \sqrt{\varepsilon_{r_g}}, \quad (1)$$

where c_0 denotes the speed of light in free space. As it appears from Fig. 2, the interaction of this wave with the metallic walls forming the shielding structure is responsible for the excitation of a diffracted field contribution, resulting in two different wavefronts W_{g_1} and W_{a_1} . The time of arrival of such radio signal changes with the angle of observation in the ground and air regions, as

$$t_{g_1} \simeq t_0 + \frac{D_c}{2c_0} \sqrt{\varepsilon_{r_+}} + \frac{\sqrt{r^2 + \frac{D_c^2}{4} - rD_c \cos \theta}}{c_0} \sqrt{\varepsilon_{r_g}} \quad (2)$$

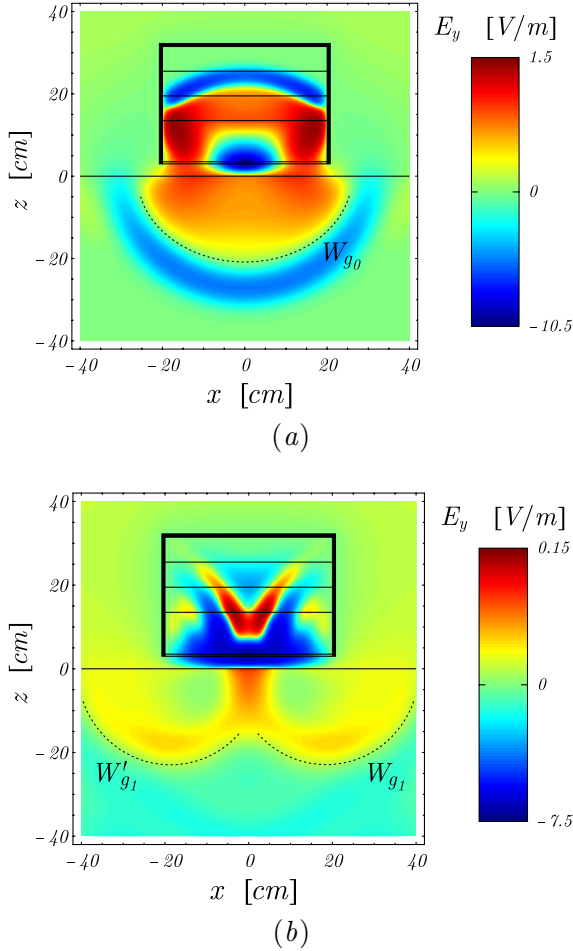


Fig. 2. Spatial distribution of the electric field excited along the H -plane of the cavity-backed resistively-loaded bow-tie antenna at the normalized time $t/\tau_g = 17.5$ (a), and $t/\tau_g = 35$ (b). The antenna is elevated over a homogeneous ground with electrical properties $\epsilon_{r_g} = 6$ and $\sigma_g = 0.015 \text{ S/m}$. The radiation process from the feed, as well as the diffraction phenomena arising from the field interaction with the cavity can be noticed.

and

$$t_{a_1} \simeq t_0 + \frac{D_c}{2c_0} \sqrt{\epsilon_{r_+}} + \frac{\sqrt{r^2 + \frac{D_c^2}{4}} - r D_c \cos \theta}{c_0}, \quad (3)$$

respectively. The diffracted field then propagates back to the feed point, generating secondary undesired emission/diffraction phenomena with wavefronts W_{g_2} and W_{a_2} . This process repeats and results in the well-known *ringing* ef-

fect. This information can be usefully employed to optimize the antenna performance in realistic *GPR* surveys in terms of clutter rejection.

III. THE NEAR-FIELD ANTENNA PERFORMANCE

The goal of this study is to analyze antenna radiation properties in the near-field region, and the spatial distribution of the radiated electromagnetic field in the ground. Furthermore, the impact of different loading profiles on the total radiation level is analyzed.

Field radiation processes from the antenna in the near-zone have been investigated for three different loading profiles: $\sigma_0 = 10 \text{ S/m} < \frac{3}{4}\sigma_{opt}$, $\sigma_0 = \sigma_{opt}$, and $\sigma_0 = 100 \text{ S/m} > \sigma_{opt}$. The goal of this study was to analyze the impact of different loading profiles on the total radiation level and the focusing of the electromagnetic field into the ground. From Fig. 3, it appears that at low frequencies (e.g., $f = 100 \text{ MHz}$) variations of the loading profile parameter result in considerable variations of the radiated downwards electric field (differences are of about 10 dB). However, starting from $f \simeq 200 \text{ MHz}$, variations of the loading profile do not cause significant differences in the magnitude of the radiated field. It, also, means that the antenna efficiency is not considerably affected by the resistive loading profile that, on the other hand, plays an important role in the impedance matching property of the antenna. As it appears in Fig. 3, the surface waves level excited at the air-ground interface decreases with frequency. Consequently, the parasitic coupling processes in the antenna pair configuration may be expected to be maximum at low frequency because of the reduced electrical size of the radiating structure.

In the higher frequency band, several higher-order modes can propagate inside the metallic cavity, and each mode is characterized by a specific guided wavelength and, consequently, radiation angle into the ground. Such phenomenon can be observed in the field map shown in Fig. 3c. Furthermore, Fig. 4 clearly demonstrates the effectiveness of the shielding structure in reducing the spurious energy emission level in the

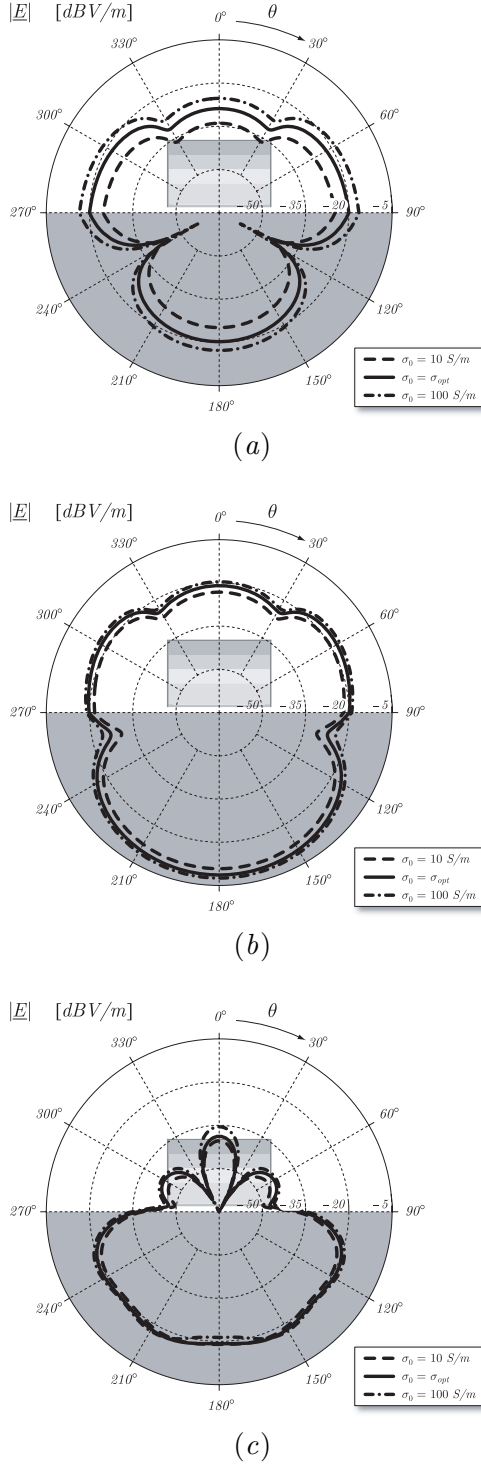


Fig. 3. H – plane near-field radiation pattern of the cavity-backed resistively-loaded bow-tie antenna at frequency $f = 100$ MHz (a), $f = 200$ MHz (b), $f = 1$ GHz (c). The observation points are located along a circle of radius $r_o = 40$ cm centered at the projection of the feeding point on the air-ground interface.

air region, as well as enhancing the antenna performance in terms of near-field front-to-back radiation ratio, defined as follows

$$FBR(r_o) = 20 \log \frac{|\underline{E}(0, 0, -r_o)|}{|\underline{E}(0, 0, r_o)|}, \quad (4)$$

denoting r_o the observation distance from the projection of the feeding point on the air-ground interface. As it can be inferred, such parameter is conveniently introduced to quantify electromagnetic field focusing properties of the antenna. In Fig. 4, we can notice that the shielded antenna is characterized by a reduced back-radiation level, which is at least 9 dB be-

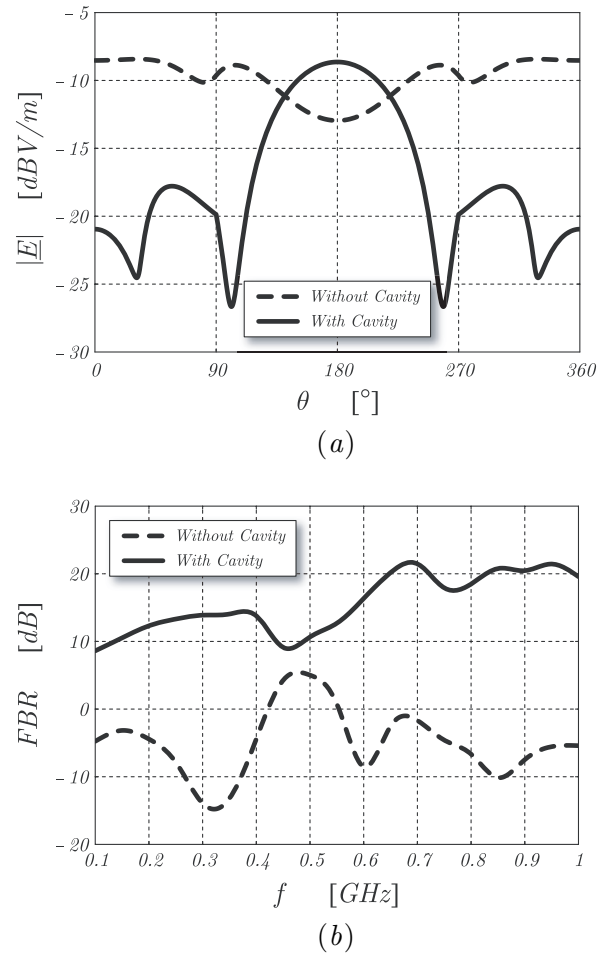


Fig. 4. Effect of the shielding cavity on the H – plane radiation pattern at 200 MHz (a), and the front-to-back radiation ratio (b) of the antenna. The observation distance from the projection of the feeding point on the air-ground interface is $r_o = 40$ cm .

low the peak value of the radio signal propagating in the soil over the whole operational frequency band. This in turn is useful to reduce potential electromagnetic interferences with nearby sensitive electronic equipment.

To analyze the electromagnetic field transmitted into the ground, the subsurface antenna footprint at a depth of 15 cm has been also computed at frequencies $f = 100 \text{ MHz}$, $f = 200 \text{ MHz}$, and $f = 1 \text{ GHz}$. The antenna footprint, representing the spot illuminated by the antenna on the ground surface or subsurface, plays an important role in GPR applications. In fact, as indicated by Daniels [4], radar imaging can be improved when the shape and size of footprint are comparable to those of the targets. When a footprint is too large it gives rise to subsurface clutter. On the other hand, a too small footprint makes the detection of buried objects difficult because of the reduced strength of the target response in a radar survey (B -scan). An optimal footprint is, also, important to improve target localization. For long targets like buried pipes or cables, it is desired to have a footprint with elongated shape, whereas for circular targets such as landmines, a footprint with circular shape would be preferred.

Figure 5 demonstrates that the electric field transmitted by the antenna in the ground is mainly polarized along the y -axis (in E -plane of the antenna). In particular, the peak level of the normalized cross-polar field component $E_x/|E_T|_{\max}$ at a depth of 15 cm is found to be below -9.5 dB over the whole operational frequency band, from 100 MHz to 1 GHz. In Fig. 5, one can also notice that the -3dB subsurface footprint of the considered antenna features a quasi-elliptical shape with semi-axes a_x , a_y directed along the coordinate axes. It results that $a_x < a_y$ at low frequency ($f \lesssim 200 \text{ MHz}$), meaning that the footprint exhibits an elongated shape along the y -axis, which would be suitable for detecting and locating long objects. The effective footprint assumes a nearly circular shape ($a_x \simeq a_y$) at $f \simeq 200 \text{ MHz}$, where the antenna efficiency and the energy level transmitted by the radiating element into the ground are maximum. Such mode

of operation is to be preferred for detection of circular-symmetric targets. Moreover, as in this case the largest size of the footprint is obtained, the mentioned operating frequency is well suited to perform a quick scan over a large area. In the high-frequency band ($f \gtrsim 200 \text{ MHz}$) a_x tends to be greater than a_y , mainly due to the effect of higher-order modes excited in the metallic cavity. As a result, the footprint tends to become elongated along the x -axis, which is useful to improve localization of long objects as in the low-frequency operation mode. In conclusion, Fig. 5 shows the footprint adaptation capability of the proposed antenna in the frequency domain with respect to the size and shape of the targets. Moreover, it's worth noting that higher operating frequency causes the radar footprint to concentrate in a reduced area near the feeding point. This information can be usefully employed to optimize the localization of small buried objects, as well as to improve the performance of detection algorithms in terms of clutter rejection.

IV. THE IMPACT OF THE GROUND

The goal of this study is to analyze the impact of the ground on circuitual and radiation properties of the antenna. This, also, includes analysis of the antenna performance for different elevations above the air-ground interface.

The circuitual characteristics of the antenna with optimal loading profile ($\sigma_0 = \sigma_{opt}$) have been analyzed in detail for different subsurface conditions (see Fig. 6). In particular, the proposed radiating element has been assumed to be elevated over sandy soil ($\varepsilon_{rg} = 4$, $\sigma_g = 0.004 \text{ S/m}$), asphalt ($\varepsilon_{rg} = 6$, $\sigma_g = 0.015 \text{ S/m}$), and dry clay ($\varepsilon_{rg} = 16$, $\sigma_g = 0.03 \text{ S/m}$). It can be noticed that the antenna is well matched to the feeding line starting from the frequency $f_\ell \simeq 55 \text{ MHz}$. Due to resistive loading and dielectric embedding, the antenna input impedance as well as the lowest operational frequency f_ℓ are only slightly affected by the very different operative conditions (see Fig. 6). On the other hand, the ground is responsible for a minor loading effect of the antenna in the low-frequency band,

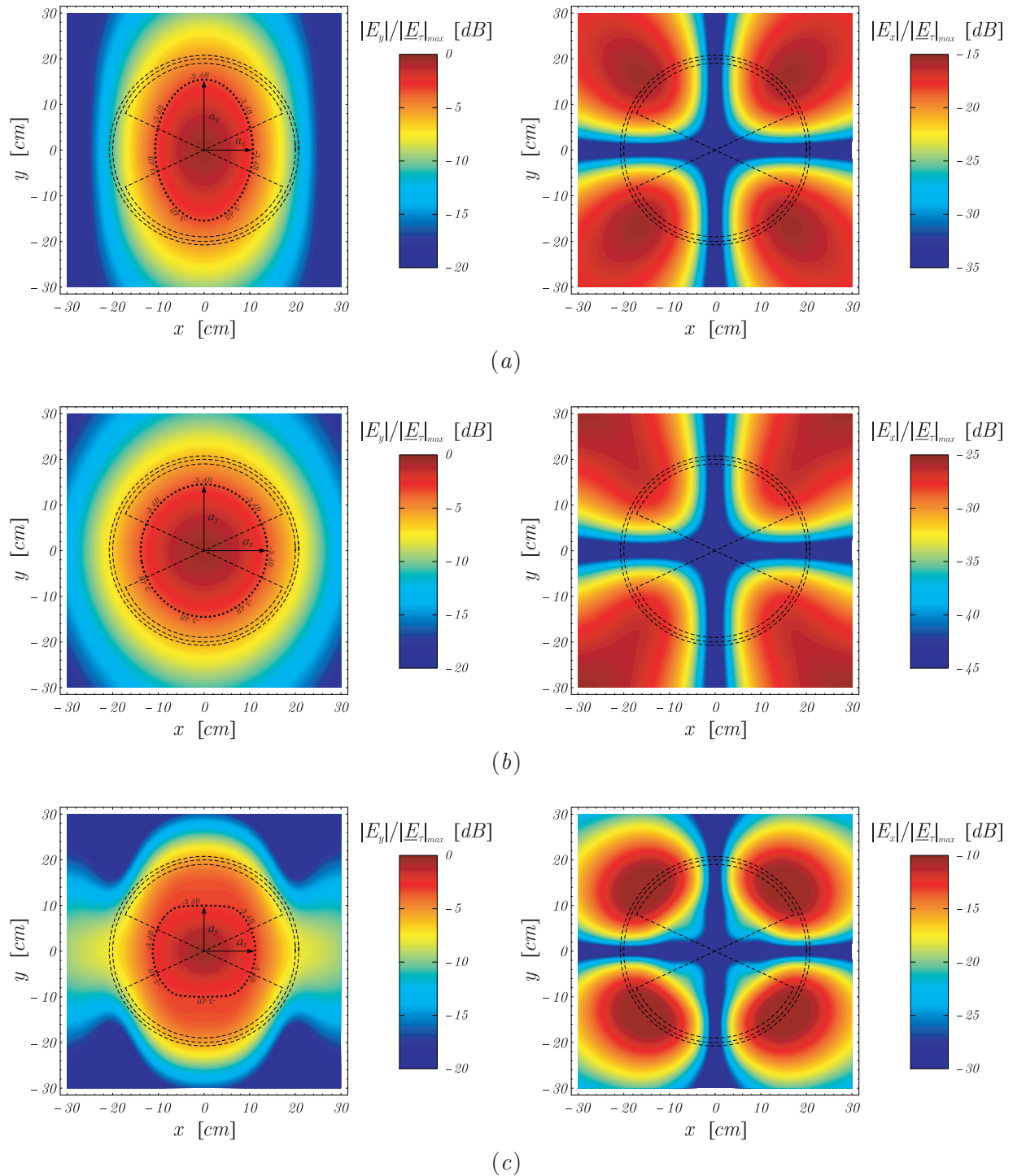


Fig. 5. Normalized subsurface antenna footprints at 15 cm depth inside the ground. Frequency: $f = 100\text{ MHz}$ (a), $f = 200\text{ MHz}$ (b), $f = 1\text{ GHz}$ (c). The antenna is elevated over a ground modeled as a homogeneous half space with electrical properties $\varepsilon_{r_g} = 6$ and $\sigma_g = 0.015\text{ S/m}$.

where the absorbing property of soil plays a significant role to reduce the level of spurious reflections and, consequently, the fluctuations in the impedance curves. Moreover, when the soil changes from *soft* ground (e.g. sand) to *hard* ground (e.g. clay), the footprint tends to become more compact in the H -plane of the antenna (x -direction), as it clearly appears from Fig. 7.

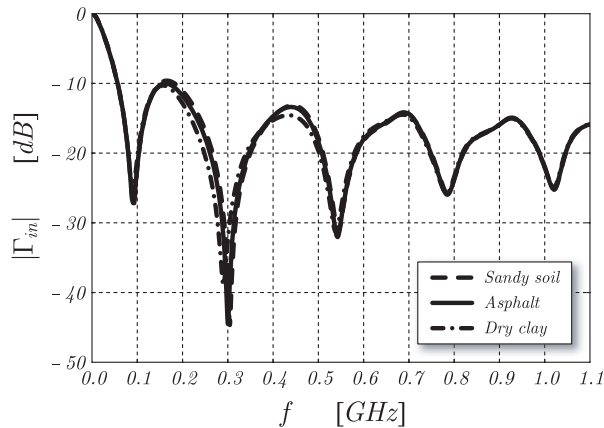


Fig. 6. Frequency behavior of the input reflection coefficient of the cavity-backed resistively-loaded bow-tie antenna for different electrical properties of the ground. The antenna is elevated 3 cm over the air-ground interface.

The input impedance of the considered radiating structure as function of the elevation above ground has been also evaluated. The computed results are given in Figs. 8 and 9. As it can be noticed in Fig. 8, the influence of the antenna elevation on the frequency behavior of the relevant input reflection coefficient is very significant only for close proximity to the interface. In particular, the smaller the distance from the interface, the better the impedance matching of the antenna to the feeding line due to the additional resistive loading effect of the lossy ground. The antenna elevation, also, has impact on the structure performance in terms of radiated power level, and radar footprint. In Fig. 9, one can observe that decreasing the distance of the radiator from the air-ground interface generally leads to a flattening of the subsurface footprint in the E -plane of the antenna (y -direction). Moreover, as it appears from Fig. 10, the amount of energy coupled into the ground tends to increase as the el-

evation over the soil becomes smaller, while reducing the parasitic back-radiation level in the air region. This information should be properly taken into account in a *GPR* survey in order to enhance the radar detection of buried targets.

V. THE RADAR DETECTION OF BURIED DIELECTRIC PIPES

In this section, emphasis is devoted to the analysis of detectability of an infinitely-long buried dielectric pipe by the subsurface radar unit consisting of two identical cavity-backed resistively-loaded bow-tie antennas (see Fig. 11). The coupling level between the transmit and receive antennas is a critical parameter in *GPR* design limiting detectability of buried targets. In the considered configuration, the transmit (T_x) antenna, denoted as antenna #1, emits a Gaussian electromagnetic pulse that propagates into the ground, where it interacts with the target, modeled as a y -directed circular cylin-

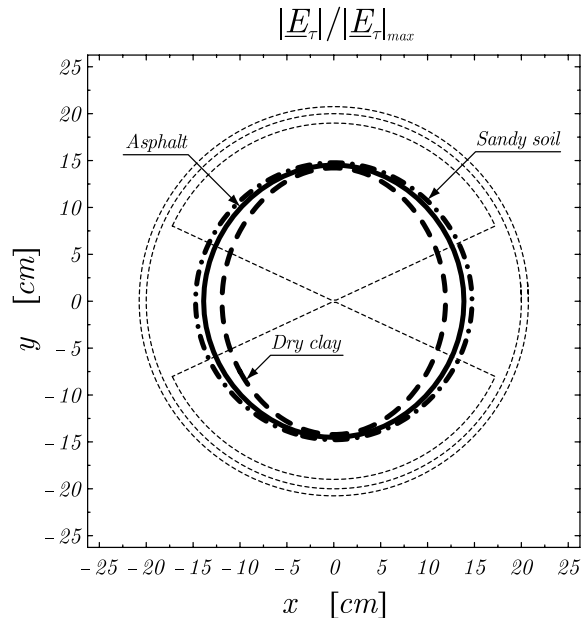


Fig. 7. Normalized -3 dB subsurface antenna footprint at 15 cm depth for different ground characteristics. The operating frequency is $f = 200\text{ MHz}$, where the antenna efficiency and the energy level transmitted into the ground are maximum. The antenna is elevated 3 cm over the air-ground interface.

der having diameter $D_p = 20\text{ cm}$, buried at a depth $h_p = 50\text{ cm}$. This interaction results in a diffracted electromagnetic field which is measured by the receive element (Rx) of the radar, denoted as antenna #2. By changing the location of the radar on the soil interface and recording the output of the receive antenna as function of time (or frequency) and radar location, one obtains the scattering data, which can be processed to get an image of the subsurface.

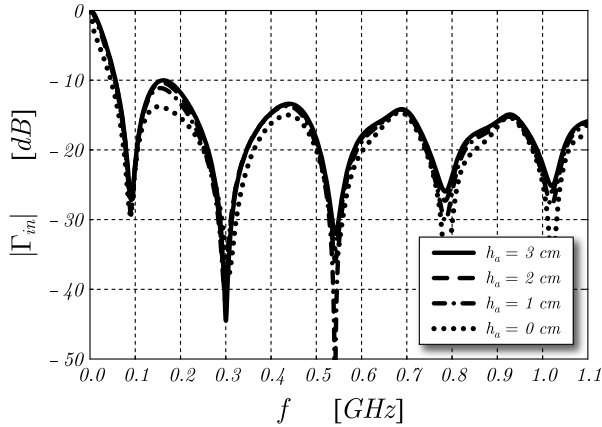


Fig. 8. Frequency behavior of the input reflection coefficient of the cavity-backed resistively-loaded bow-tie antenna as function of the elevation above ground, modelled as a lossy homogeneous half-space having relative permittivity $\epsilon_{r_g} = 6$ and electrical conductivity $\sigma_g = 0.015\text{ S/m}$.

Since the considered structure is reciprocal and symmetrical (see Fig. 11), the relevant scattering matrix \underline{S} is completely described in terms of the S_{11} and S_{21} parameters, whose evaluation is carried out by feeding the radiating element #1, and setting the excitation signal of the antenna #2 equal to zero.

As it appears from Fig. 12, the return loss of the transmit antenna is negligibly affected by the buried target that, at the same time, has a reduced impact on the S_{21} parameter. This means that the antenna coupling is mainly responsible for the received signal. It is worth mentioning that the maximum coupling level is a decreasing function of antenna separation, d_a , and tends to become larger as the relative permittivity of the pipe ϵ_{r_p} increases

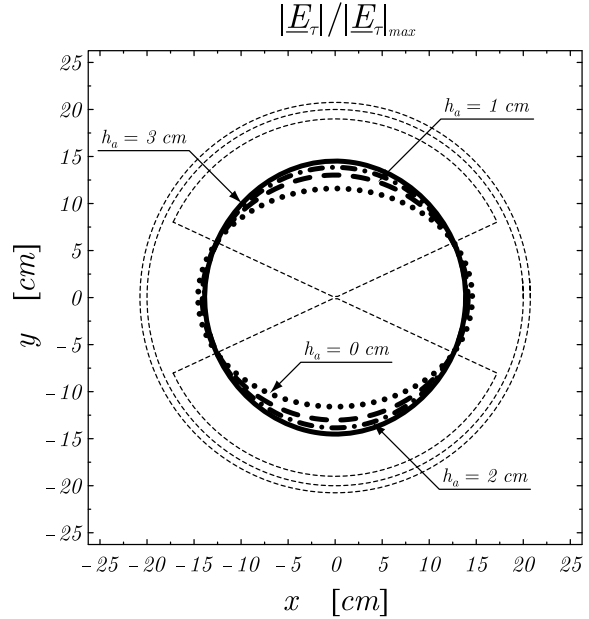


Fig. 9. Normalized -3 dB subsurface antenna footprint at 15 cm depth for different elevations above ground. The operating frequency is $f = 200\text{ MHz}$.

(see Fig. 12). In particular, for an antenna separation $d_a = 5\text{ cm}$, the coupling level is below -30 dB over the whole operational frequency band $100\text{ MHz} - 1\text{ GHz}$. The effect of the antenna elevation above the ground, h_a , has been also investigated, although the relevant analysis is not reported here for sake of brevity. It has been found that, as h_a decreases, the antenna return-loss response is slightly shifted towards lower frequencies because of the proximity effect of the soil. On the other hand, the ground influence on the S_{21} parameter is noticeable only at high frequencies, where the mutual coupling level decreases as the radiating elements approach the air-ground interface.

As it can be noticed in Fig. 13, the peak-to-peak level of the voltage contribution v_{d_2} due to the presence of the pipe, excited at the input terminals of the receive antenna, is essentially function of the difference between relative permittivities of the ground and the pipe, namely the dielectric contrast $\Delta\epsilon_r = \epsilon_{r_g} - \epsilon_{r_p}$, and is about one order of magnitude smaller than the peak-to-peak level of the voltage contribution v_{r_2} due to direct antenna coupling, un-

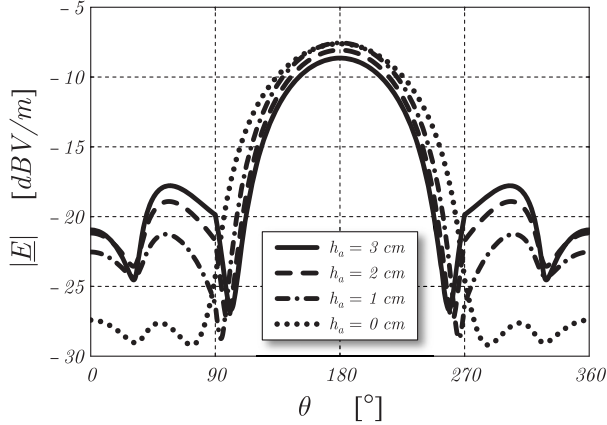


Fig. 10. H - plane radiation pattern at 200 MHz of the resistively-loaded bow-tie antenna for different elevations over the soil. The observation distance from the projection of the feeding point on the air-ground interface is $r_o = 40\text{ cm}$.

der the assumption that the depth of the buried target is $h_p = 50\text{ cm}$. The spectrum of the radio signal arising from the subsurface diffraction is similar to the spectrum of the direct coupling, and the relevant largest spectral contribution is given by the frequency harmonics around 200 MHz , the frequency around which the direct coupling reaches its maximum. It should be noticed that parasitic antenna coupling can potentially result in the early-time masking of the buried target. So, to reduce or possibly prevent such problem, it is of crucial importance in a *GPR* design to adopt an antenna system with a short in time direct coupling response, and reduced decaying factor. In particular, it has been numerically found that the exponential decaying factors of v_{d_2} and v_{r_2} are, for the considered antenna pair configuration, $\tau_{d_2} \simeq 2.766\text{ ns}$ and $\tau_{r_2} \simeq 2.518\text{ ns}$, respectively.

It is worth noting that, where the dielectric contrast of the buried pipe $\Delta\epsilon_r$ is negative, a phase inversion occur in the diffracted field distribution and, consequently, in the relevant radio signal component detected by the receiver. This results in interference phenomena responsible for a significant downward focalization of the total field, as outlined in Fig. 14. Such information can be usefully employed to optimize the detec-

tion of buried pipes in subsurface radar applications, as well as to enhance the performance of detection algorithms in terms of clutter rejection.

VI. CONCLUSION

We have investigated the performance of a novel cavity-backed loaded bow-tie antenna which has been designed for a new ground penetrating radar. The considered radiating structure shows an outstandingly large operational

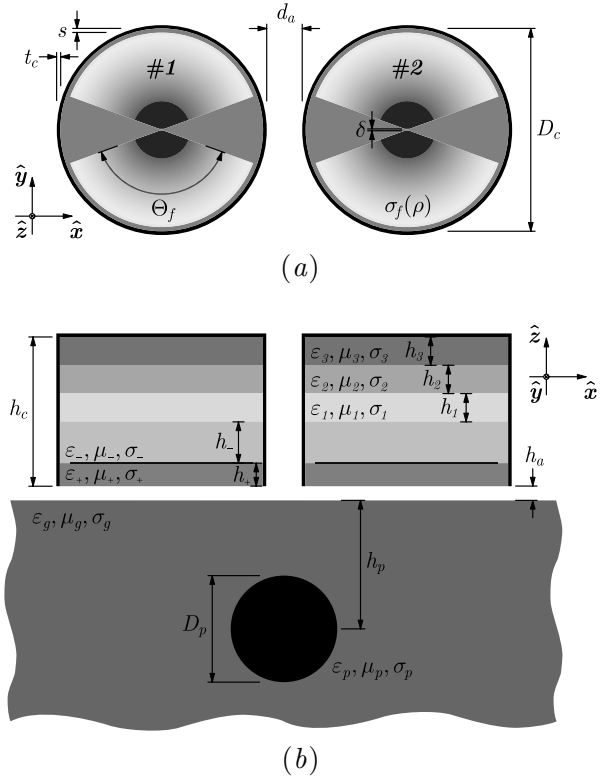


Fig. 11. Bottom (a) and cross-sectional (b) view of a subsurface radar unit consisting of two identical cavity-backed resistively-loaded bow-tie antennas located above a lossy homogeneous half space where an infinitely-long dielectric pipe is buried. Structure characteristics: $D_c = 40\text{ cm}$, $s = 1\text{ cm}$, $t_c = 0.5\text{ cm}$, $\Theta_f = 130^\circ$, $\delta = 0.25\text{ cm}$, $h_c = 28.5\text{ cm}$, $h_a = 3\text{ cm}$, $\epsilon_{r_g} = 6$, $\sigma_g = 0.015\text{ S/m}$, $h_+ = 0.5\text{ cm}$, $\epsilon_{r_+} = 3$, $\sigma_+ = 0\text{ S/m}$, $h_- = 10\text{ cm}$, $\epsilon_{r_-} = 10$, $\sigma_- = 0\text{ S/m}$, $h_1 = 6\text{ cm}$, $\epsilon_{r_1} = 11$, $\sigma_1 = 0.125\text{ S/m}$, $h_2 = 6\text{ cm}$, $\epsilon_{r_2} = 15$, $\sigma_2 = 0.25\text{ S/m}$, $h_3 = 6\text{ cm}$, $\epsilon_{r_3} = 20$, $\sigma_3 = 1\text{ S/m}$, $d_a = 5\text{ cm}$, $h_p = 50\text{ cm}$, $D_p = 20\text{ cm}$.

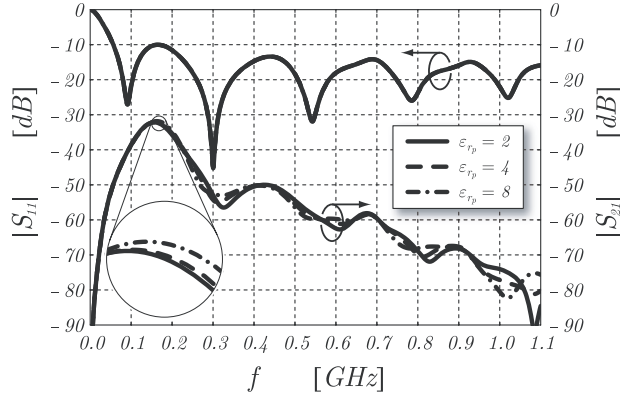


Fig. 12. Frequency behavior of the scattering parameters of the cavity-backed resistively-loaded bow-tie antenna pair for different permittivities of the buried pipe, having electrical conductivity $\sigma_p = 0.01 \text{ S/m}$. The antenna separation is assumed to be $d_a = 5 \text{ cm}$.

bandwidth from 55 MHz to $>1.5 \text{ GHz}$ combined with a maximal size of 40 cm .

The circuitual and radiation characteristics of the antenna with optimal loading profile have been investigated in detail for different subsurface conditions. The ground is responsible for a minor loading effect of the structure in the low-frequency band, where the absorbing property of soil plays a significant role to reduce the level of spurious reflections and, consequently, the fluctuations in the impedance curves. Similar minor

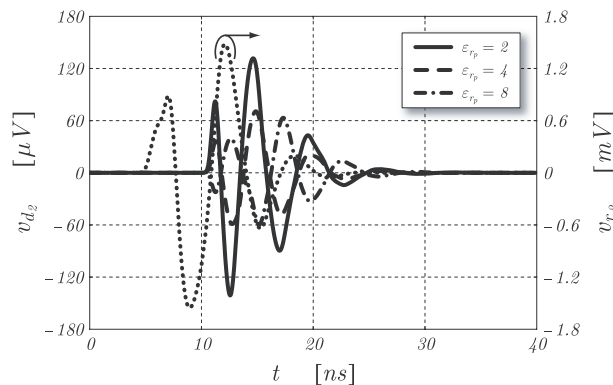


Fig. 13. Transient voltages at the receiver due to the direct coupling between antennas, and scattering from a buried dielectric pipe having relative permittivity ε_{rp} and electrical conductivity $\sigma_p = 0.01 \text{ S/m}$.

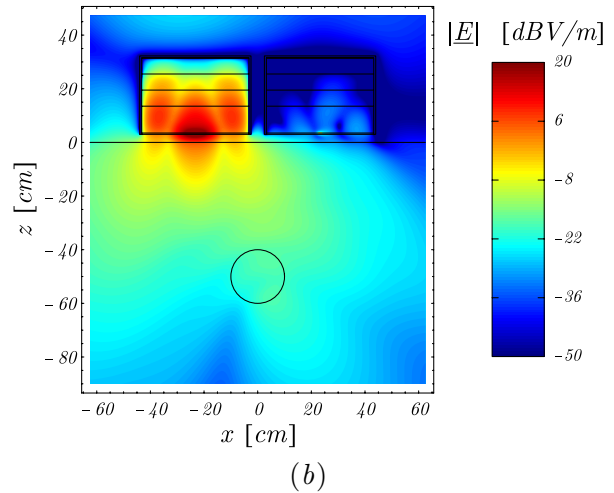
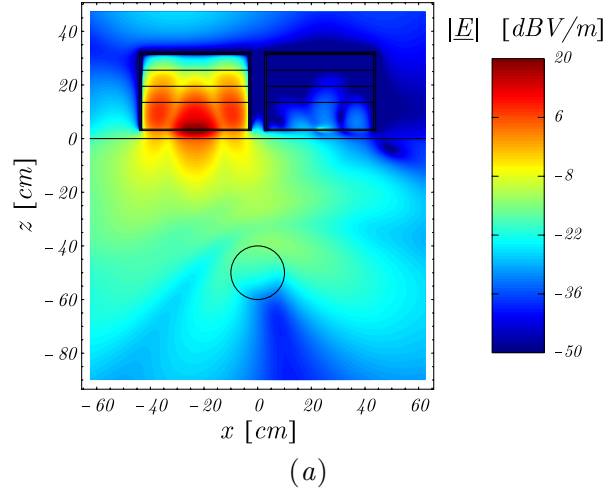


Fig. 14. Spatial distribution of the electric field excited along the vertical cut-plane of the antenna pair operating in presence of a buried dielectric pipe having relative permittivity $\varepsilon_{rp} = 2$ (a) and $\varepsilon_{rp} = 8$ (b). Operational frequency: $f = 500 \text{ MHz}$.

variations in the impedance curves have been observed by variations of the structure elevation above the ground. Antenna radiation properties in the near-field region are, also, only slightly affected by the ground. In particular, when the soil changes from *soft* ground (e.g. sand) to *hard* ground (e.g. clay), the antenna footprint tends to become slightly more compact. In general, the antenna clearly demonstrates ground invariant behavior, which is of ultimate importance for synthesis of time-domain pulses in *SFCW* radar applications.

The analysis of near-field radiation processes has shown a reasonably good transient behavior of the antenna, which simplifies the task of deconvolution of the antenna impulse response from the measured *SFCW* data. This behavior makes it possible to use the developed antenna in a time-domain radar. An interesting footprint adaptation capability of the proposed antenna in the frequency domain with respect to the size and shape has been observed. Such property can be usefully adopted to improve the radar detection of buried targets in a *GPR* survey. Also, the antenna exhibits relatively high value for the front-to-back radiation ratio and reduced spurious energy emission level in the air region, which allows for increase of the total output power of the radar transmitter without breaching allowed (e.g., by *FCC* regulations) radiation levels.

A particular attention has been devoted to the analysis of detectability of buried pipes by the subsurface radar unit consisting of two identical antennas. It has been found that the direct coupling level between transmit and receive antennas is below -30 dB over the whole operating frequency band from 100 MHz to 1 GHz. In particular, the exponential decaying factor of the radio signal contribution at the receiver end due to the parasitic antenna coupling is reasonably small. Such feature is particularly important in order to reduce the early-time masking of the target in a *GPR* survey. The waveform and magnitude of received signals due to scattering from buried dielectric pipes have been also investigated. The obtained numerical results have provided a useful physical insight into antenna mutual coupling, and scattering from buried targets. This information is required to evaluate the required *GPR* dynamic range where the maximal received signal is due to the antenna coupling and the minimal detectable signal should be smaller than the weakest reflection from a thin dielectric pipe on the maximal expected depth.

ACKNOWLEDGMENT

This research has been carried out in the framework of EU-sponsored project *ORFEUS* (contract number: *FP6-2005-Global-4-036856*).

The authors would like to thank anonymous reviewers for their suggestions and comments.

REFERENCES

- [1] D. Caratelli, A. G. Yarovoy, and L. P. Ligthart, "Design and full-wave analysis of cavity-backed resistively loaded circular-end bow-tie antennas for GPR applications – Part I," accepted for publication in *ACES Journal*, 2010.
- [2] D. Caratelli, "Full-wave analysis of cavity-backed resistively loaded bow-tie antennas for GPR applications," Delft University of Technology, the Netherlands, Tech. Rep. IRCTR-S-001-08, Jan. 11, 2008.
- [3] D. Caratelli, A. Yarovoy, and L. P. Ligthart, "Full-wave analysis of cavity-backed resistively loaded bow-tie antennas for GPR applications," *European Microwave Conference 2008*, Amsterdam, the Netherlands, pp. 204-207, October 27-31, 2008.
- [4] D. Daniels, *Ground Penetrating Radar*, 2nd ed., IEE Press, 2004.
- [5] A. A. Lestari, A. G. Yarovoy, and L. P. Ligthart, "Numerical and experimental analysis of circular-end wire bow-tie antennas over a lossy ground," *IEEE Trans. Antennas Propagat.*, vol. 52, pp. 26-35, Jan. 2004.
- [6] Y. Nishioka, O. Maeshima, T. Uno, and S. Adachi, "FDTD analysis of resistor-loaded bow-tie antennas covered with ferrite-coated conducting cavity for subsurface radar," *IEEE Trans. Antennas Propagat.*, vol. 47, pp. 970-977, June 1999.
- [7] D. Uduwawala, M. Norgren, P. Fuks, and A. W. Gunawardena, "A deep parametric study of resistor-loaded bow-tie antennas for ground-penetrating radar applications using FDTD," *IEEE Trans. Geosci. Remote Sensing*, vol. 42, pp. 732-742, Apr. 2004.
- [8] K.-H. Lee, C.-C. Chen, F. L. Teixeira, and R. Lee, "Modeling and investigation of a geometrically complex UWB GPR antenna using FDTD," *IEEE Trans. Antennas Propagat.*, vol. 52, pp. 1983-1991, Aug. 2004.
- [9] L. Gürel and U. Oguz, "Simulations of ground-penetrating radars over lossy and heterogeneous grounds," *IEEE Trans. Geosci. Remote Sensing*, vol. 39, pp. 1190-1197, June 2001.
- [10] L. Gürel and U. Oguz, "Optimization of the transmitter-receiver separation in the ground-

penetrating radar,” *IEEE Trans. Antennas Propagat.*, vol. 51, pp. 362-370, Mar. 2003.



Diego Caratelli was born in Latina, Italy on May 2, 1975. He received the Laurea (summa cum laude) and Ph.D. degrees in Electronic Engineering from “La Sapienza” University of Rome, Italy in 2000 and 2004, respectively. In 2005, he joined as a Contract Researcher the Department of Electronic Engineering, “La Sapienza” University of Rome. Since 2007, he is with the International Research Centre for Telecommunications and Radar (*IRCTR*) of Delft University of Technology, the Netherlands, as a Senior Researcher.

His main research activities include the design, analysis and experimental verification of printed microwave and millimeter-wave passive devices and wideband antennas for satellite, *WLAN* and *GPR* applications, the development of analytically based numerical techniques devoted to the modeling of electromagnetic field propagation and diffraction processes, as well as the analysis of *EMC/EMI* problems in sensitive electronic equipment.

Dr. Caratelli was the recipient of the 2010 Young Antenna Engineer Prize at the 32th European Space Agency Antenna Workshop. He is a member of the Italian Electromagnetic Society (*SIEm*).



Alexander G. Yarovoy (M’96-SM’04) graduated from the Kharkov State University, Ukraine, in 1984 with the Diploma with honor in radiophysics and electronics. He received the Candidate Phys. & Math. Sci. (Ph.D. equivalent) and Doctor Phys. & Math. Sci. (D.Sc. equivalent) degrees in radiophysics in 1987 and 1994, respectively.

In 1987, he joined the Department of Radiophysics at the Kharkov State University as a Researcher and became a Professor there in 1997. From September 1994 through 1996, he was with Technical University of Ilmenau, Germany as a Visiting Researcher. Since 1999, he is with the International Research Centre for Telecommunications-Transmission and Radar (*IRCTR*) at the Delft University of Technology, the Netherlands. Since 2009, he leads there a chair of Microwave Technology and Systems for Radar. His main research interests are in ultra-wideband (*UWB*) microwave technology and its applications (in particular, *UWB* radars) and applied electromagnetics (in particular, *UWB* antennas).

Prof. Yarovoy is the recipient of a 1996 International Union of Radio Science (*URSI*) “Young Scientists Award” and the European Microwave Week Radar Award in 2001 for the paper that best advances the state-of-the-art in radar technology (together with L.P. Ligthart and P. van

Genderen). Prof. Yarovoy served as the Chair of the 5th European Radar Conference (*EuRAD’08*), Amsterdam, The Netherlands, and Co-Chairman and the Technical Program Committee Chair of the Tenth International Conference on Ground Penetrating Radar (*GPR2004*), Delft.